Research Article

Advances in Mechanical Engineering

Advances in Mechanical Engineering
2016, Vol. 8(9) 1–14

DOI: 10.1177/1687814016670284
aime.sagepub.com
SAGE

Surface grinding of carbon fiber–reinforced plastic composites using rotary ultrasonic machining: Effects of tool variables

Hui Wang[1], Fuda Ning[1], Yingbin Hu[1], PKSC Fernando[2], ZJ Pei[2] and Weilong Cong[1]

Abstract

Carbon fiber–reinforced plastic composites have many superior properties, including low density, high strength-to-weight ratio, and good durability, which make them attractive in many industries. However, due to anisotropic properties, high stiffness, and high abrasiveness of carbon fibers in carbon fiber–reinforced plastic, high cutting force, high tool wear, and high surface roughness are always caused in conventional machining processes. This article reports an investigation using rotary ultrasonic machining in surface grinding of carbon fiber–reinforced plastic composites in order to develop an effective and high-quality surface grinding process. In rotary ultrasonic machining surface grinding of carbon fiber–reinforced plastic composites, tool selection is of great importance since tool variables will significantly affect output variables. In this work, the effects of tool variables, including abrasive size, abrasive concentration, number of slots, and tool end geometry, on machining performances, including the cutting force, torque, and surface roughness, are experimentally studied. The results show that lower cutting forces and torque are generated by the tool with higher abrasive size, lower abrasive concentration, and two slots. Lower surface roughness is generated by the tool with smaller abrasive size, smaller abrasive concentration, two slots, and convex end geometry. This investigation will provide guides for tool selections during rotary ultrasonic machining surface grinding of carbon fiber–reinforced plastic composites.

Keywords

Surface grinding, carbon fiber–reinforced plastic composite, rotary ultrasonic machining, tool variable, tool selection

Date received: 27 June 2016; accepted: 29 August 2016

Academic Editor: Xichun Luo

Introduction

Carbon fiber–reinforced plastic (CFRP) composites consist of carbon fiber and polymer. Carbon fiber is used to support the load, and polymer is used to transmit the load to carbon fibers and to bind and protect the fibers.[1] CFRP composites have a variety of superior properties, such as high strength-to-weight ratio, high elastic modulus, good durability, low thermal expansion coefficient, and high corrosion resistance.[2–9] Due to these attractive properties, CFRP composites have been widely used in

[1]Department of Industrial Engineering, Texas Tech University, Lubbock, TX, USA
[2]Department of Industrial and Manufacturing Systems Engineering, Kansas State University, Manhattan, KS, USA

Corresponding author:
Weilong Cong, Department of Industrial Engineering, Texas Tech University, Lubbock, TX 79409, USA.
Email: weilong.cong@ttu.edu

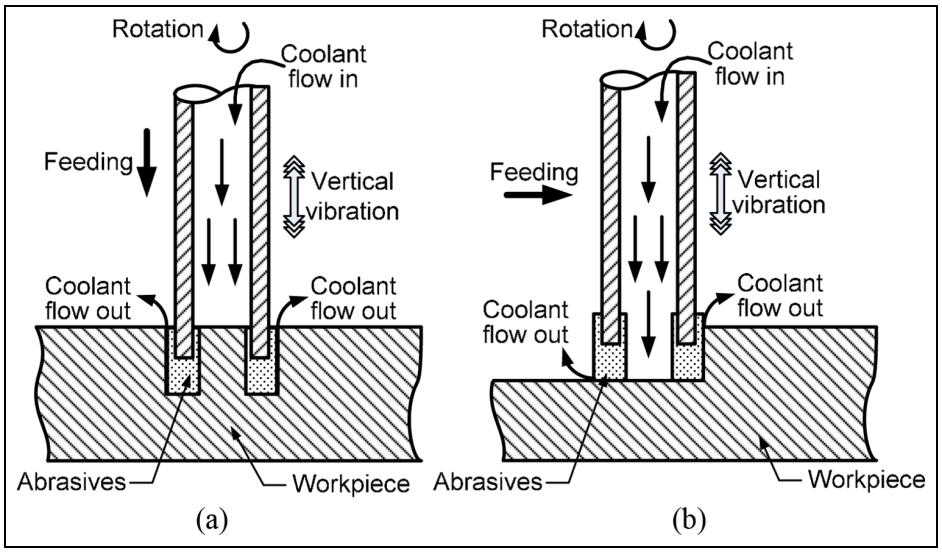

Figure 1. Illustration of rotary ultrasonic machining: (a) rotary ultrasonic hole making and (b) rotary ultrasonic surface grinding.

many industries, such as aerospace, automobile, electronics, medical device, and sports.[2,9–12]

The near-net-shaped parts can be fabricated after CFRP composites' molding processes.[13,14] Additional machining processes, including hole making and surface/edge machining, are still required to obtain the desired tolerances, dimensional precision, and shape in order to meet the application requirement including fitting and joining.[13,15–18] During the assembly, the workpieces often need to be drilled for joining.[19] Surface machining also plays an important role in obtaining the final quality of CFRP composites.[3,4,19,20] Surface machining processes, such as grinding and milling, are used to remove a small amount of materials to generate functional surfaces with good surface quality and high dimensional accuracy.[4] Compared with surface milling, surface grinding can produce even better surface quality and higher dimensional accuracy.[4,7,8] However, the problems of traditional surface grinding still exist in some aspects, including high cutting force, high tool wear, high surface roughness, and high cutting temperature.[3,4,7,9] It became critical to find an effective, efficient, and high-quality surface machining process for solving these problems. This article reports on such a surface machining process: rotary ultrasonic machining (RUM).

It was reported that RUM could generally decrease the cutting force, cutting temperature, tool wear, surface roughness, and workpiece delamination in CFRP composites' hole making.[21–32] RUM surface grinding has been used in machining of many materials, including ceramics, silicon, titanium alloys, medium carbon steels, as well as CFRP composites.[33–41] However, there are no reported investigations on the effects of tool variables on output variables in RUM surface grinding of CFRP composites. RUM material removal mechanisms consist of ultrasonic machining and traditional grinding process. During RUM machining, the rotating tool vibrates at an ultrasonic frequency (typically 20 kHz). The cutting tool feeds toward the workpiece at a constant feedrate along its axial direction for RUM hole making (as illustrated in Figure 1(a)) or along the top surface of the workpiece for RUM surface grinding (as illustrated in Figure 1(b)). The coolant is pumped through the core of the grinding tool to wash away the swarf and prevent the tool from overheating.

In RUM surface grinding of CFRP composites, tool selection is very important since tool variables will significantly affect output variables. However, there are no reported investigations on the effects of tool variables in such a process. The investigation in this article for the first time studies the effects of tool variables (including abrasive size, abrasive concentration, number of slots, and tool geometry) on output variables (including the cutting forces in both feeding direction and axis direction, torque, and surface roughness) of the process. The investigations on RUM surface grinding of CFRP composites with different tool variables will be beneficial to tool selection for future research.

This article consists of four sections. After the "Introduction" section, workpiece properties, experimental setup, and measurement procedures are described in the second section. And then the experimental results are presented in the third section. Finally, conclusions are drawn in the fourth section.

Workpiece properties, experimental setup, and measurement procedures

Workpiece properties

The CFRP composite workpieces used in this investigation were composed of plain woven carbon fibers and

Table 1. Properties of workpiece material.

Property	Unit	Value
Density of CFRP	kg/m^3	1544
Hardness (Rockwell)	HRB	62–67
Density of carbon fiber	kg/m^3	1800
Density of epoxy matrix	kg/m^3	1200
Elastic modulus of carbon fiber	GPa	230
Elastic modulus of epoxy matrix	GPa	4.5
Tensile strength of carbon fiber	GPa	5
Tensile strength of epoxy matrix	MPa	130
Poisson's ratio of carbon fiber	–	0.3
Poisson's ratio of epoxy matrix	–	0.4
Fracture toughness of carbon fiber (energy/G_c)	J/m^2	2
Fracture toughness of epoxy matrix (energy/G_c)	J/m^2	500

CFRP: carbon fiber–reinforced plastic.

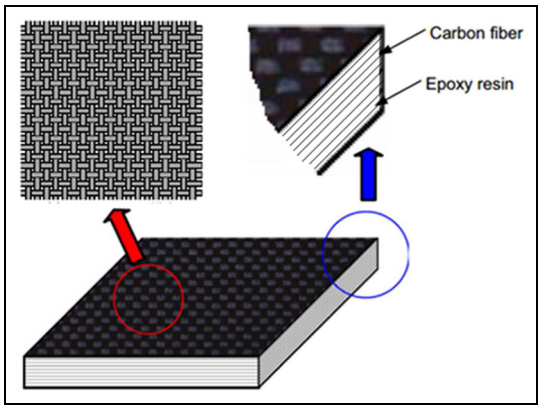

Figure 2. Fiber structures in CFRP.

epoxy resin matrix, as illustrated in Figure 2. They all had 10 layers of carbon fabric with the 0°/90° orientation of the carbon fiber yarn in the woven structure. The size of the workpiece was 326 mm × 20 mm × 6 mm. The properties of the CFRP composite workpiece material are listed in Table 1.

Experimental setup

The experiments of this investigation were performed on a rotary ultrasonic machine (Series 10; Sonic-Mill, Albuquerque, NM, USA). As shown in Figure 3, the RUM experimental setup includes an ultrasonic spindle system, a coolant system, and a data acquisition (DAQ) system. The ultrasonic spindle system was composed of ultrasonic power supply, ultrasonic spindle, and motor with rotation-speed controller. The ultrasonic power supply was used to convert low-frequency (60 Hz) line electricity to the constant high-frequency (20 kHz) electrical energy. The frequency of the ultrasonic vibration was fixed and maintained at 20 kHz. The ultrasonic power supply could control the amplitude of the ultrasonic vibration through input power percentage. The high-frequency electrical energy was supplied to the piezoelectric converter (located inside the ultrasonic spindle) to be converted into high-frequency mechanical vibration (ultrasonic vibration). The ultrasonic vibration was then transmitted to the grinding tool through ultrasonic spindle. The rotation motion of the spindle was provided by the motor which was assembled on the top of ultrasonic spindle. The coolant system, composed of pressure regulator and gauges, values, flow rate, pump, and coolant tank, provided coolant to the spindle and the interface between the tool and the workpiece. The DAQ system was used to collect experimental data during the experiments. More detailed information for this DAQ system will be discussed in measurement procedures.

To achieve the surface grinding feeding motion, a horizontal feeding system was setup, as shown in Figure 4. The horizontal feeding motion was supplied by a linear stage (D-slide 400 mm; Newmark, Rancho Santa Margarita, CA, USA) and the feedrate was controlled by a motor controller (NSC-A1; Newmark) and a software (QuickMotion NSC-A1; Newmark). Both the workpiece and the dynamometer were fixed on the platform of the linear stage.

Measurement procedures

Cutting force and torque. The DAQ system shown in Figure 3 was used for the cutting force and torque measurement. The cutting force in the horizontal feeding direction (F_x), the cutting force in the vertical axis direction (F_z), and the torque were measured by a dynamometer (Type 9272; Kistler Inc., Winterthur, Switzerland). The electrical signals from the dynamometer were amplified by a charge amplifier (Type 5070; Kistler Inc.). After that, the amplified electrical signals were transformed into digital signals by the analog-to-digital (A/D) converter (Type 5697A; Kistler Inc.). The digital signals were acquired by a computer with the help of DynoWare software (Type 2825D-02; Kistler Inc.).

In the RUM process, the cutting force changed with time and the fluctuation was in a certain range. Figure 5 shows the typical cutting force in the feeding direction (F_x) fluctuating with time in RUM surface grinding. There are three major sections in this curve. Once the cutting tool touched the workpiece, the cutting force kept increasing until the tool was fully fed into the workpiece (as shown in section (a) of Figure 5). Section (b) in Figure 5 covered the process with the tool fully fed into the workpiece. If the cutting tool started leaving the workpiece, the cutting force kept decreasing to 0, as shown in section (c) of Figure 5. The cutting

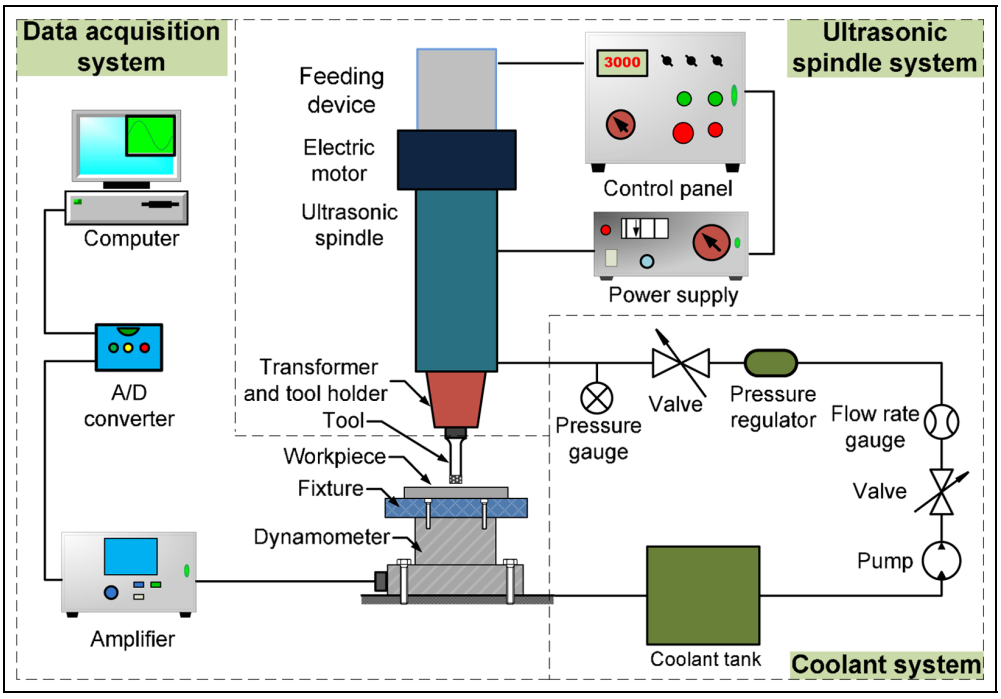

Figure 3. Rotary ultrasonic machining (RUM) experimental setup.

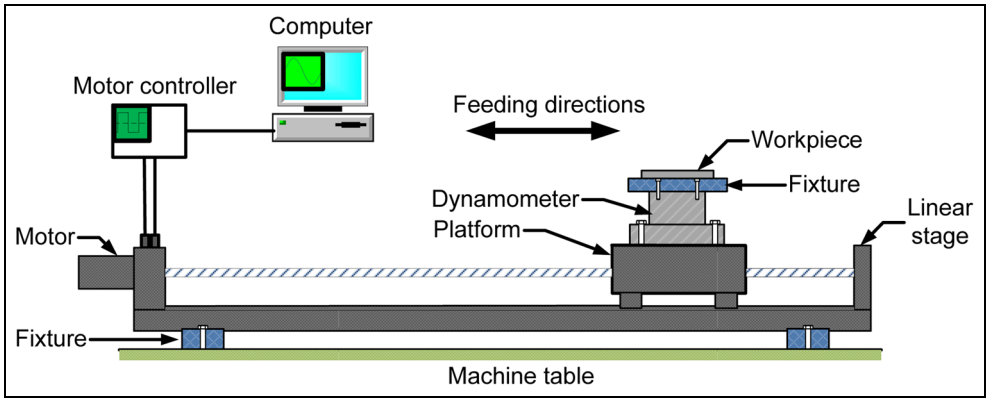

Figure 4. Horizontal feeding system setup.

force used in the investigation is the average value in section (b) of Figure 5. Similar reading methodology will also be used in obtaining the cutting force in the axis direction (F_z) and torque.

Surface roughness. A surface profilometer (Surftest-402; Mitutoyo Corporation, Kanagawa, Japan) was used to measure surface roughness. The test range and cut-off length were set at 4 and 0.8 mm, respectively. The average surface roughness value (R_a) was used in this investigation. As shown in Figure 6, four positions were selected for the measurement of surface roughness. Two of them located in the cutting entrance area, and the other two located in the exit area. Each measurement was repeated three times in each position.

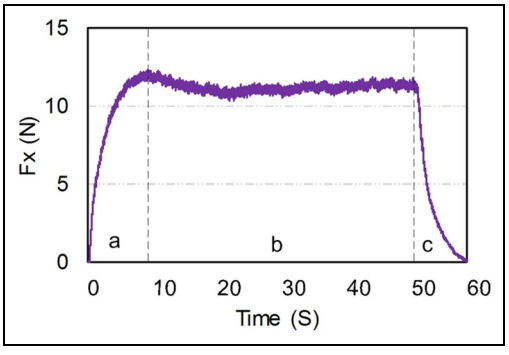

Figure 5. Typical curve of cutting force in feeding direction (F_x) versus cutting time. (Section a: the tool was feeding into the workpiece; section b: the tool fully fed into the workpiece; section c: the tool was leaving the workpiece.).

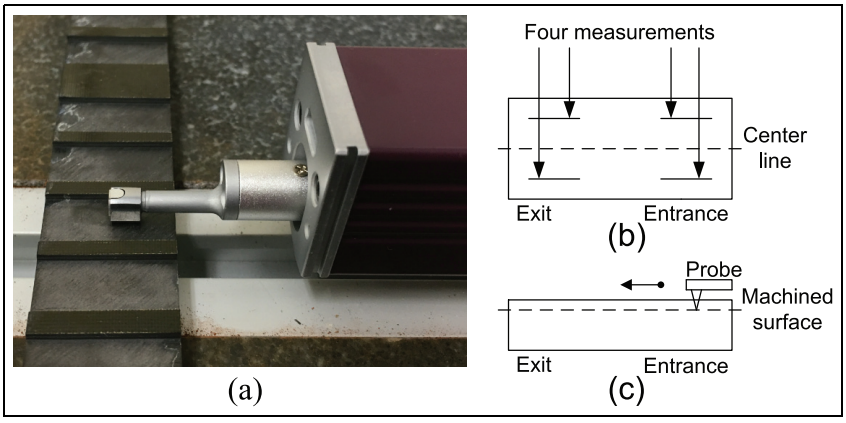

Figure 6. Measurements of surface roughness: (a) measurement setup, (b) top view, and (c) side view.

Table 2. Tool parameters.

Tools	Geometry (Figure 6)	AMS (mesh#)	AS d (mm)	Slots (#)	AC (%)	OD (mm)	ID (mm)	TL (mm)
Tool #1	a	60/80	0.20	0	100	12.7	10.5	51
Tool #2	a	80/100	0.16	0	100	12.7	10.5	51
Tool #3	a	120/140	0.12	0	100	12.7	10.5	51
Tool #4	a	80/100	0.16	0	75	9.525	7.7	45
Tool #5	a	80/100	0.16	0	100	9.525	7.7	45
Tool #6	a	80/100	0.16	0	100	9.525	7.7	45
Tool #7	b	80/100	0.16	2	100	9.525	7.7	45
Tool #8	c	80/100	0.16	4	100	9.525	7.7	45
Tool #9	d	80/100	0.16	0	100	9.525	5	45
Tool #10	e	80/100	0.16	0	100	9.525	5	45
Tool #11	f	80/100	0.16	0	100	9.525	5	45

AMS: abrasive mesh size; AS: abrasive size; AC: abrasive concentration; OD: outside diameter; ID: inner diameter; TL: tuning length.

Table 3. Experimental conditions and tool variables.

	Variables	Unit	Values	Tool geometry
Machining parameters (fixed)	Tool rotation speed, *S*	r/min	3000	
	Feedrate, F_r	mm/s	0.4	
	MRR	mm^3/s	5.08 (For tool #1–3); 3.81 (for tool #4–11)	
	Ultrasonic power, *W*	%	40% (400 W)	
	Operating frequency	kHz	20	
	Tool amplitude	μm	12	
Tool variables	Abrasive size, *As*	mm	0.12, 0.16, 0.20	a
	Concentration, *Ca*		75, 100	a
	Number of slots		0, 2, 4	a, b, c
	Geometry, *G*		Flat, concave, convex	d, e, f

MRR: material removal rate.

Cutting tools and experimental conditions

The metal bonded diamond grinding tools were used in surface grinding of CFRP composites using RUM. The detailed tool variables are listed in Tables 2 and 3. These cutting tools can be classified into four groups: (1) tools with different abrasive sizes (as shown in Table 2), (2) tools with different abrasive concentrations (as shown in Table 2), (3) tools with different numbers of slots (as shown in Figure 7(a)–(c)), and (4) tools with different end geometries (as shown in Figure 7(d)–(f) and Table 2).

The experimental conditions are listed in Table 3. In the experiment, machining variables (include tool rotation speed, feedrate, material removal volume, and ultrasonic power) were kept the same. The machining

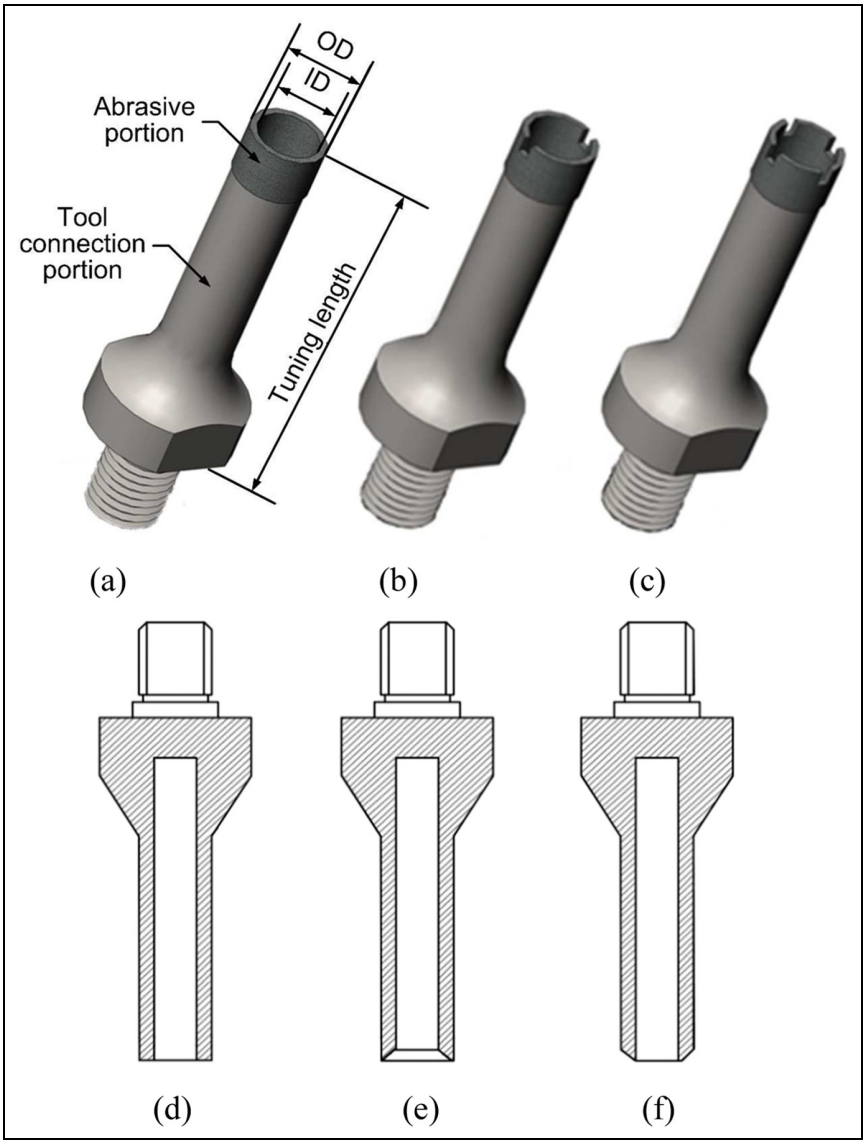

Figure 7. Tools with different geometries: (a) the tool without slots, (b) the tool with two slots, (c) the tool with four slots, (d) the flat tool, (e) the concave tool, and (f) the convex tool.

process was performed three times under each machining condition.

Experimental results and discussion

Effects on cutting force

The effects of tool variables (including abrasive size, abrasive concentration, number of slots, and tool geometry) on the cutting forces in both the feeding direction (F_x) and the axial direction (F_z) were investigated.

Effects of abrasive size. Figure 8 shows the effects of abrasive size on both F_x and F_z. Both F_x and F_z decreased with the increase in abrasive size. F_x was always higher than F_z and had larger variation than F_z. The largest abrasive size also generated the largest difference between F_x and F_z. The relationship between the cutting forces and abrasive size agreed with other reported trends in surface grinding processes of CFRP[7] and RUM drilling processes.[30]

The number of abrasive grains, participating in machining, on the outside face and end face of RUM tool can be obtained by equations (1) and (2), respectively[27]

$$n_x = \left[\frac{0.88 \times 10^{-3}}{(\pi/6)d^3\rho}\frac{C_a}{100}\right]^{\frac{2}{3}} A_{0x} \quad (1)$$

$$n_z = \left[\frac{0.88 \times 10^{-3}}{(\pi/6)d^3\rho}\frac{C_a}{100}\right]^{\frac{2}{3}} A_{0z} \quad (2)$$

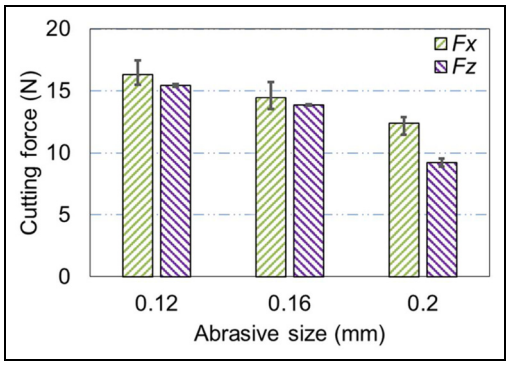

Figure 8. Effects of abrasive size on cutting force.

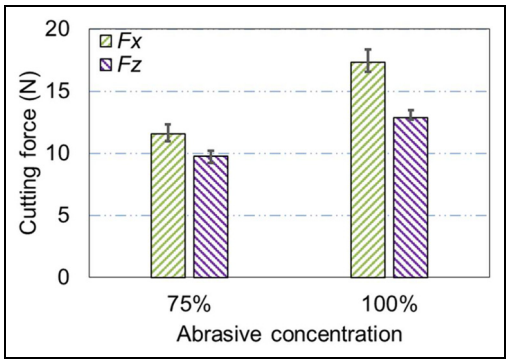

Figure 9. Effects of abrasive concentration on cutting force.

where n_x and n_z are the numbers of abrasive grains on the outside face and end face of RUM tool, respectively; C_a is the abrasive concentration; d is the abrasive size (diameter in millimeter); ρ is the material density of abrasive grain (g/mm^3), $\rho = 3.52 \times 10^{-3}$ g/mm^3 for diamond; A_{0x} and A_{0z} are the outside-face and end-face areas of the cutting tool, respectively (mm^2), $A_{0x} = \pi D_0 \times DoC$ and $A_{0z} = \pi({D_0}^2 - {D_i}^2)/4$ (D_o is the outer diameter of RUM tool, mm; D_i is the inner diameter of the tool, mm; and DoC is the depth of cut, mm). It can be seen from equations (1) and (2) that the number of abrasive grains on both the outside face and end face of the tool decreases with the increase in abrasive size.

The relationship between F_x and F_z and the number of abrasive grains participating in machining can be obtained from equations (3) and (4), respectively[27,30,37]

$$F_x = n_x F_{1x} \tag{3}$$

$$F_z = n_z \Delta t f F_{1z} \tag{4}$$

where Δt is the effective cutting time (s); f is the ultrasonic frequency (Hz); F_{1x} and F_{1z} are the average cutting forces for one grain in the feeding and axial directions, respectively (N).

As can be seen from equations (1) and (2), the increase in abrasive-grain diameter caused the decrease in the number of active grains participating in machining on both the outside and end faces. Because total material removal rate (MRR) was kept the same (5.08 mm^3/s), the average MRR for one grain (MRR_1) was increased, leading to the increase in both F_{1x} and F_{1z} forces.[3,42–46] With equations (3) and (4), the decrease rate of active abrasive-grain number might be larger than the increase rate of F_{1x} or F_{1z} forces, leading to the decrease in the cutting forces.[27,30,37]. In addition, it was also reported that in general grinding process, the smaller abrasive grain has faster wear rate, leading to the increase in the cutting forces.[43,47,48]

Effects of abrasive concentration. The effects of abrasive concentration on the cutting forces in both the feeding direction (F_x) and the axial direction (F_z) are shown in Figure 9. It can be seen that compared with abrasive concentration of 75 (54 carats of diamond grains are in per cubic inch[49]), using RUM tool with abrasive concentration of 100 (72 carats of diamond grains are in per cubic inch[49]) resulted in both higher F_x and higher F_z. For each tool, F_x was always higher and had larger variation than F_z. The tool with abrasive concentration of 100 generated larger difference between F_x and F_z. The trends agreed with the cutting force model (F_z) for RUM drilling of the brittle materials.[27,30]

It can be seen from equations (1) and (2) that with an increase in abrasive concentration, the number of grains participating in machining increased. Comparing to the tool with abrasive concentration of 75, the tool with abrasive concentration of 100 had larger number of active grains participating in machining. Since the total MRR was kept the same (3.81 mm^3/s), the one-grain MRR_1 was smaller for the tool with abrasive concentration of 100, resulting in the decrease in indentation depth δ and then the decrease in effective contact time (one grain), leading to decreased F_{1z},[30] and the decrease in one-grain MRR_1 also caused the decrease in F_{1x}.[3,42–46] In equations (3) and (4), the effects of the increase in the number of abrasive grains participating in machining might have overridden the effects of the decrease in F_{1x} or F_{1z}, resulting in an increase in the cutting force.[27,30,37] Another possible reason was that comparing to the tool with abrasive concentration of 75, the tool with abrasive concentration of 100 had larger total cutting contact between the tool and the workpiece, resulting in the increase in the mechanical load and then the increase in the cutting forces (F_x and F_z).[50] In RUM surface grinding of CFRP, larger total cutting contact between the tool and the workpiece led to increased grinding chips, diamond and resin bond debris from tool, and then higher friction force between the tool and the workpiece, resulting in higher cutting forces.[48]

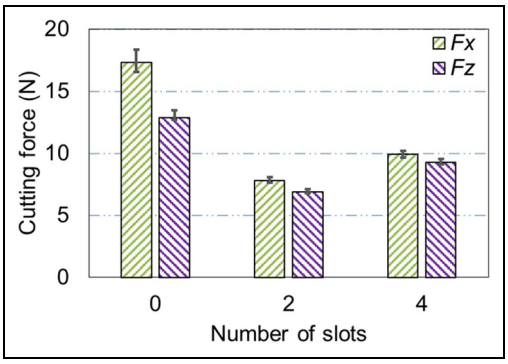

Figure 10. Effects of number of slots on cutting force.

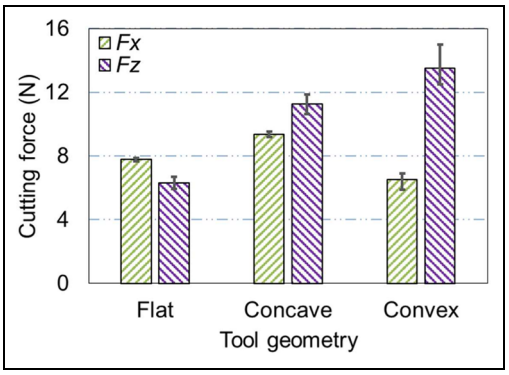

Figure 11. Effects of tool geometry on cutting force.

Effects of number of slots. The effects of the number of slots on the cutting forces can be seen from Figure 10. Both F_x and F_z first decreased and then increased with the increase in the number of slots. They both reached the lowest when using two-slot cutting tool and the highest when using no-slot cutting tool. In general, comparing with the tools without slots, the tools with slots could decrease both F_x and F_z. For each tool, F_x was always higher than F_z. The tool without slots had larger variation in both F_x and F_z and generated larger difference between F_x and F_z.

The possible reason was that the tool without slots had the largest number of abrasive grains participating in machining on both the outside and end faces of the tool. When the total MRR was kept the same, the larger number of active abrasive grain caused the smaller one-grain MRR_1, leading to lower F_1 (F_{1x} and F_{1z}). However, the effects of the increase in the number of active abrasive grains might have overridden the effects of the decrease in F_{1x} or F_{1z}, resulting in the cutting forces using the tool without slots being higher than using the two-slot or four-slot tools.[27,30,37] Another possible reason was that more active abrasive grains led to larger active cutting contact, resulting in higher cutting forces in both the directions (F_x and F_z).[50] In addition, the slots on the tools would increase the coolant flow rate, decreasing the friction force at the interface between the tool (end face and outside face) and the workpiece. For this reason, both F_x and F_z were decreased when the tools with slots were used. Comparing with the two-slot tool, the four-slot tool had less abrasive grains participating in machining, leading to higher tool wear and one-grain MRR_1 (the total MRR was the same, $3.81\,mm^3/s$) and then resulting in higher F_{1x} and F_{1z}.[3,43–48] Using equations (3) and (4), the increase rate of F_{1x} and F_{1z} might play a more important role than the decreasing rate of active abrasive-grain numbers, resulting in the cutting forces using the four-slot tool being higher than using the two-slot tool.[27,30,37]

Effects of tool geometry. The effects of tool geometry on both F_x and F_z are shown in Figure 11. It can be seen from Figure 11 that the concave tool generated the highest F_x and the convex tool generated the lowest F_x. For F_z, the highest value was found in RUM using the convex tool and the lowest was obtained in RUM using the flat tool. For both the convex and concave tools, F_z forces were higher than F_x forces; however, the flat tool had opposite relationship. The convex tool caused the largest variation in both F_x and F_z and the largest difference between F_x and F_z.

In this experiment, the areas of tools participating in machining included the outside and end faces. The outside-face areas were 29.92, 29.92, and $48.7\,mm^2$ for the flat tool, concave tool, and convex tool, respectively. The end-face areas were 51.62, 7.64, and $4.12\,mm^2$ for the flat tool, concave tool, and convex tool, respectively. During this experimental investigation, to keep the total MRR the same ($3.81\,mm^3/s$), the depth of cut (1.4 mm) using the convex tool was larger than that (1 mm) using the flat or concave tool. The depth of cut played a dominant role in F_z, and larger depth of cut resulted in higher F_z force.[3,45–46] In addition, larger friction force was generated between the outside face of the convex tool and the workpiece. With this case, F_z force generated from the convex tool was the highest among these three kinds of tools.

Comparing to the flat or convex tools, the concave tool had smaller number of grains taking part in machining processes, causing larger one-grain MRR_1 (as well as F_{1x}) and higher tool wear. In equation (3), the decreased rate of the number of active abrasive grains might have smaller influence on F_x than the increase in F_{1x}, resulting in using the concave tool generating the highest F_x.[27,30,37] In addition, it can be seen from Figure 12 that when using the convex tool, the cutting force perpendicular to the major cutting contacting interface could be divided into two parts, F'_x ($F\cos\alpha$) and F'_z ($F\sin\alpha$). However, when using the flat

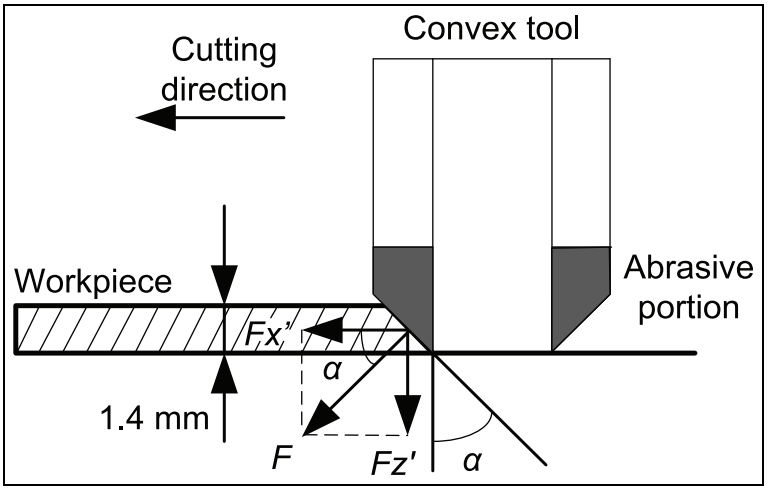

Figure 12. Illustration of convex tool in RUM surface grinding.

or concave tool, the cutting force perpendicular to the major cutting contacting interface was F_x. This was the possible reason why F_x generated by the convex tool was the lowest.

Effects on torque

The torque was correlated with the cutting forces in both the directions (F_x and F_z) in machining and equaled to the cutting force by moment arm of force. In this investigation, it was shown from Figures 13–16 that the changing trends of the torque were consistent with those of the cutting forces in the axial direction, F_z. This result agreed with all formal investigations in RUM hole making of CFRP composites and stainless steel. The explanations of the effects on the cutting forces can also be used to explain the effects on the torque.[23,24,31,32,51,52]

Effects of abrasive size. Figure 13 shows the effects of abrasive size on the torque. It can be seen that the larger abrasive size generated higher torque and torque variation in RUM surface grinding of CFRP.

Effects of abrasive concentration. The relationship between abrasive concentration and torque is illustrated in Figure 14. It is shown that compared with the tool with abrasive concentration of 75, the tool with abrasive concentration of 100 generated higher torque and torque variation in RUM surface grinding of CFRP.

Effects of number of slots. Figure 15 illustrates the effects of the number of slots on the torque. It is shown that the two-slot tool resulted in the lowest torque and torque variation, and the tool without slots caused the highest torque and torque variation in RUM surface grinding of CFRP.

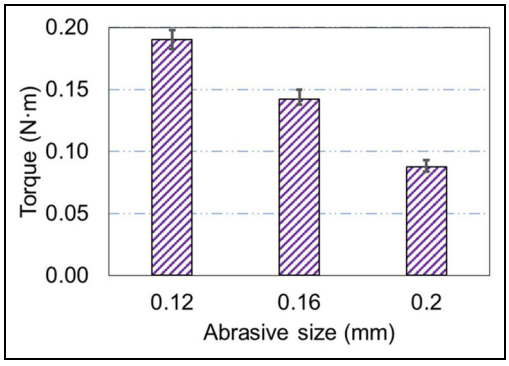

Figure 13. Effects of abrasive size on torque.

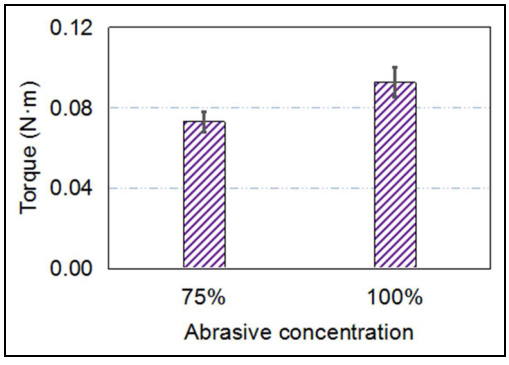

Figure 14. Effects of abrasive concentration on torque.

Effects of tool geometry. Figure 16 shows the effects of tool end geometry on the torque. It can be seen that the flat tool generated the lowest torque and torque variation, and the convex tool caused the highest torque and

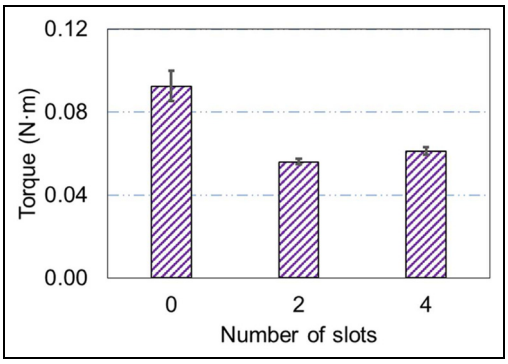

Figure 15. Effects of number of slots on torque.

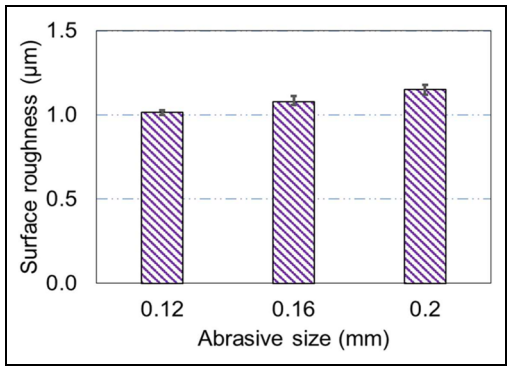

Figure 17. Effects of abrasive size on surface roughness.

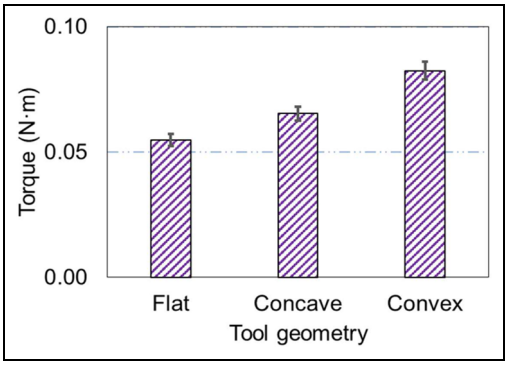

Figure 16. Effects of tool geometry on torque.

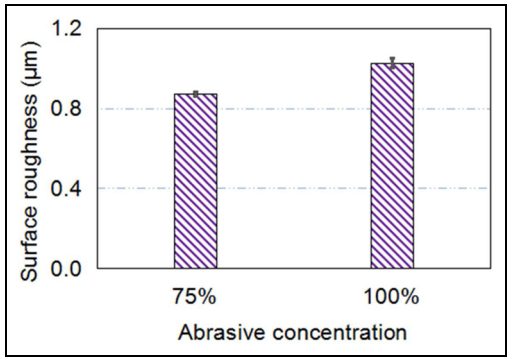

Figure 18. Effects of abrasive concentration on surface roughness.

torque variation in RUM surface grinding of CFRP. For the convex tool, the moment arm of force was lower than using the flat or concave tools. However, the increasing rate of the cutting force was much larger than the decreasing rate of arm of force, resulting in the highest torque using the convex tool.

Effects on surface roughness

The effects of tool variables (including abrasive size, abrasive concentration, number of slots, and tool geometry) on surface roughness (the average surface roughness, R_a) were investigated and are shown in Figures 17–20. The contact (including contacting force, contacting time and area, and lubrication conditions) between the tool and the workpiece will affect surface roughness.[9,36,43,50,53]

Effects of abrasive size. Figure 17 illustrates the effects of abrasive size on surface roughness. It was shown that surface roughness and its variations increased with the increase in abrasive size. The results also agreed with those in other processes, such as grinding of CFRP, steel–ceramic composites, and ceramic matrix composites, and RUM of CFRP, Ti, ceramics, and so on.[7,50,54–60]

The possible reason for R_a and its variation changes was that by equations (1) and (2), the increase in abrasive size (abrasive-grain diameter) caused the decrease in the number of active grains participating in machining on both the outside and end faces. And then it caused the decrease in the total cutting contact resulting in the increase in surface roughness. It can be interpreted by the kinematic overlap factor, which represented the overlapping of all abrasive grains' participation in grinding a specific area. The decreasing total cutting contact (larger abrasive size) caused the decrease in the kinematic overlap factor. The smaller overlap factor caused a larger surface roughness.[50] In addition, the smaller abrasive size caused smaller one-grain MRR_1, resulting in shallower wear scars, less fiber fracture, and smaller chipping length. As a result, surface roughness was decreased using the tool with smaller abrasive size.[60]

Effects of abrasive concentration. Figure 18 shows the effects of abrasive concentration on surface roughness. It can be seen that the grinding tool with abrasive concentration of 100 generated larger surface roughness R_a and its variation than the tool with abrasive concentration of 75. The relationship between abrasive concentration and surface roughness was similar to that

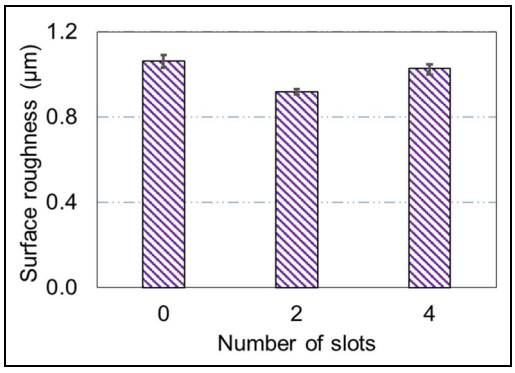

Figure 19. Effects of number of slots on surface roughness.

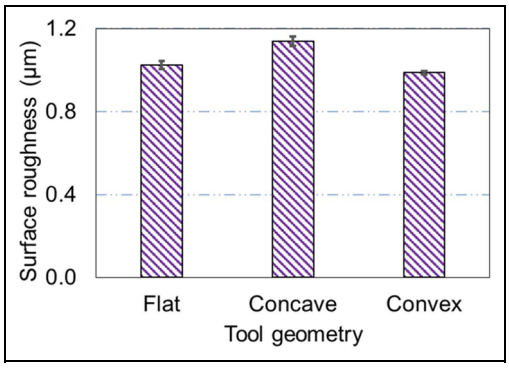

Figure 20. Effects of tool geometry on surface roughness.

between abrasive concentration and F_x. This finding was consistent with RUM of titanium alloy.[58]

The possible reason of this relationship was that the larger concentration caused larger workpiece temperature in machining.[47] The higher temperature may lead to some resin soften, resulting in larger surface roughness.[7,61] Another possible reason was that the increase in contacting force F_x caused the increase in load of the cutting tool, leading to the increase in the rate of tool wear. The CFRP composites were not sharply cut, resulting in the increase in surface roughness.[9,36] In addition, the tool with abrasive concentration of 75 had more cavities between the tool and the workpiece, and the cavities can carry coolant and clean the cutting chips. Therefore, the tool with abrasive concentration of 75 contributed to a smaller surface roughness than that with abrasive concentration of 100.

Effects of number of slots. Figure 19 shows the effects of the number of slots on surface roughness. Surface roughness first decreased and then increased with the increase in the number of slots. The two-slot cutting tool generated the smallest R_a and its variation while using the tool without slots generated the largest R_a and its variation.

The possible reason was that with the increase in contacting force F_x, the load of the cutting tool increased, leading to the increase in the tool-wear rate. Therefore, the CFRP composites were not sharply cut, resulting in higher surface roughness.[9,36] Another possible reason was that the slots on the tool would increase the coolant flow rate, which could improve the lubrication between the tool and the workpiece. For the two-slot tool, it had both enough total cutting contact (time and area) and good lubrication. Comparing to the tool without slots, although the two-slot tool had less grains participating in grinding, the coolant between the tool and the workpiece played a lubrication role in generating smaller surface roughness. For this reason, the two-slot tool led to a smaller surface roughness than that without slots.[50,59,60] Comparing with the two-slot tool, the four-slot tool had less abrasive grains taking part in grinding, resulting in the decrease in active cutting contact (time and area) and further leading to a larger R_a value.[50] In addition, the decreasing rate of the number of grains was much larger, resulting in the increase in average MRR (MRR_1) and further the increase in tool wear, which led to the increase in surface roughness.[9,36] This was the possible reason why the four-slot tool resulted in the larger surface roughness.

Effects of tool geometry. Figure 20 shows the effects of the tool geometry on surface roughness. It can be seen that the concave tool generated remarkably larger surface roughness (worse surface finish) and its variation than the flat or convex tool. The relationship between the tool geometry and surface roughness was similar to that between the tool geometry and F_x forces.

The possible reason was that the increase in the contacting force F_x generated by the concave tool caused the increase in cutting-tool load, leading to the increase in tool-wear rate. For this reason, the CFRP composites were not sharply cut, leading to the concave tool generating the highest surface roughness.[9,36] Another possible reason was that during RUM surface grinding, the flat tool and convex tool had more abrasive grains participating in machining per unit area, leading to smaller surface roughness.[50] In addition, it was also the possible reason that the flat and convex tool had better coolant conditions.

Conclusion

In this article, the effects of RUM tool variables (including abrasive size, abrasive concentration, number of slots, and tool geometry) on output variables (cutting forces, torque, and surface roughness) have been for the first time investigated in RUM surface grinding processes when MRR was kept the same. The

following conclusions can be drawn from this investigation:

1. All cutting forces (F_x and F_z) and torque decreased with the increase in abrasive size. Surface roughness increased with the increase in abrasive size.
2. The tool with larger abrasive concentration generated higher cutting forces (F_x and F_z), torque, and surface roughness.
3. With the increase in the number of slots, cutting forces (F_x and F_z), torque, and surface roughness first decreased and then increased.
4. The concave tool generated the highest F_x and surface roughness. The convex tool resulted in the lowest F_x and surface roughness and caused the highest F_z and torque. The flat tool generated the lowest F_z and torque.
5. The changing trends of torque were consistent with those of the cutting force in axial direction F_z.

This article studied the effects of different kinds of tools on surface grinding of CFRPs using RUM and provided guides for future investigations, especially for tool selections during RUM surface grinding of CFRPs. More experiments need to be conducted to investigate tool variables with dominant effects on different output variables.

Declaration of conflicting interests

The author(s) declared no potential conflicts of interest with respect to the research, authorship, and/or publication of this article.

Funding

The author(s) disclosed receipt of the following financial support for the research, authorship, and/or publication of this article: The work was supported by US National Science Foundation through award CMMI-1538381.

References

1. Black JT and Kohser RA. *DeGarmo's materials and processes in manufacturing*. 11th ed. Hoboken, NJ: John Wiley & Sons, Inc., 2012.
2. Ruegg CH and Habermeier J. Composite propeller shafts: design and optimization. *Automot Eng* 1981; 6: 13–15.
3. Hu NS and Zhang LC. A study on the grindability of multidirectional carbon fibre-reinforced plastics. *J Mater Process Tech* 2003; 140: 152–156.
4. Hu NS and Zhang LC. Some observations in grinding unidirectional carbon fiber-reinforced plastics. *J Mater Process Tech* 2004; 152: 333–338.
5. Davim JP and Reis P. Drilling carbon fiber reinforced plastics manufactured by autoclave-experimental and statistical study. *Mater Design* 2003; 24: 315–324.
6. Chung DDL. *Composite materials: science and applications*. 2nd ed. London: Springer-Verlag London Ltd, 2010.
7. Soo SL, Shyha IS, Barnett T, et al. Grinding performance and workpiece integrity when superabrasive edge routing carbon fibre reinforced plastic (CFRP) composites. *CIRP Ann: Manuf Techn* 2012; 61: 295–298.
8. Cao XY, Lin B, Wang Y, et al. Influence of diamond wheel grinding process on surface micro-topography and properties of SiO_2/SiO_2 composite. *Appl Surf Sci* 2014; 292: 181–189.
9. Sasahara H, Kikuma T, Koyasu R, et al. Surface grinding of carbon fiber reinforced plastic (CFRP) with an internal coolant supplied through grinding wheel. *Precis Eng* 2014; 38: 775–782.
10. Hintze W, Cordes M and Koerkel G. Influence of weave structure on delamination when milling CFRP. *J Mater Process Tech* 2015; 216: 199–205.
11. Zhong ZW and Hung NP. Grinding of alumina/aluminum composites. *J Mater Process Tech* 2002; 123: 13–17.
12. Wang YG, Li B, Zhang CL, et al. A simple solid-liquid grinding/templating route for the synthesis of magnetic iron/graphitic mesoporous carbon composites. *Carbon* 2013; 51: 397–403.
13. Karpat Y and Polat N. Mechanistic force modeling for milling of carbon fiber reinforced polymers with double helix tools. *CIRP Ann: Manuf Techn* 2013; 62: 95–98.
14. Hocheng H, Puw HY and Huang Y. Preliminary study on milling of unidirectional carbon fibre-reinforced plastics. *Compos Manuf* 1993; 4: 103–108.
15. Konig W, Wulf C, Graß P, et al. Machining of fibre reinforced plastics. *CIRP Ann: Manuf Techn* 1985; 34: 537–548.
16. Karakas MS, Acir A, Ubeyli M, et al. Effect of cutting speed on tool performance in milling of B_4C_p reinforced aluminum metal matrix composites. *J Mater Process Tech* 2006; 178: 241–246.
17. Karpat Y, Bahtiyar O and Deger B. Mechanistic force modeling for milling of unidirectional carbon fiber reinforced polymer laminates. *Int J Mach Tool Manu* 2012; 56: 79–93.
18. Sreenivasulu R. Optimization of surface roughness and delamination damage of GFRP composite material in end milling using Taguchi design method and artificial neural network. *Proced Eng* 2013; 64: 785–794 (also published in *international conference on design and manufacturing (IConDM2013)*).
19. Hintze W, Hartmann D and Schütte C. Occurrence and propagation of delamination during the machining of carbon fibre reinforced plastics (CFRPs): an experimental study. *Compos Sci Technol* 2011; 71: 1719–1726.
20. Hosokawa A, Hirose N, Ueda T, et al. High-quality machining of CFRP with high helix end mill. *CIRP Ann: Manuf Techn* 2014; 63: 89–92.
21. Cong WL, Feng Q, Deines T, et al. Dry machining of carbon fiber reinforced plastic composite by rotary ultrasonic machining: effects of machining variables. In: *Proceedings of the 2011 ASME international manufacturing science and engineering conference*, Corvallis, OR, 13–17 June 2011. New York: ASME.

22. Cong WL, Pei ZJ, Deines TW, et al. Rotary ultrasonic machining of CFRP using cold air as coolant: feasible regions. *J Reinf Plast Comp* 2011; 30: 899–906.
23. Cong WL, Pei ZJ, Feng Q, et al. Rotary ultrasonic machining of CFRP: a comparison with twist drilling. *J Reinf Plast Comp* 2012; 31: 313–321.
24. Cong WL, Feng Q, Pei ZJ, et al. Rotary ultrasonic machining of carbon fiber reinforced plastic composites: using cutting fluid versus cold air as coolant. *J Compos Mater* 2012; 46: 1745–1753.
25. Cong WL, Pei ZJ, Deines TW, et al. Rotary ultrasonic machining of CFRP composites: a study on power consumption. *Ultrasonics* 2012; 52: 1030–1037.
26. Feng Q, Cong WL, Pei ZJ, et al. Rotary ultrasonic machining of carbon fiber reinforced polymer: feasibility study. *Mach Sci Technol* 2012; 16: 380–398.
27. Liu DF, Cong WL, Pei ZJ, et al. A cutting force model for rotary ultrasonic machining of brittle materials. *Int J Mach Tool Manu* 2012; 52: 77–84.
28. Liu DF, Tang YJ and Cong WL. A review of mechanical drilling for composite laminates. *Compos Struct* 2012; 94: 1265–1279.
29. Cong WL, Pei ZJ, Deines TW, et al. Rotary ultrasonic machining of CFRP/Ti stacks using variable feedrate. *Compos Part B: Eng* 2013; 52: 303–310.
30. Cong WL, Pei ZJ, Sun X, et al. Rotary ultrasonic machining of CFRP: a mechanistic predictive model for cutting force. *Ultrasonics* 2014; 54: 663–675.
31. Ning FD and Cong WL. Rotary ultrasonic machining of CFRP: design of experiment with a cutting force model. In: *Proceedings of the ASME 2015 international manufacturing science and engineering conference*, Charlotte, NC, 8–12 June 2015, paper no. MSEC2015-9227. New York: ASME.
32. Ning FD, Cong WL, Pei ZJ, et al. Rotary ultrasonic machining of CFRP: a comparison with grinding. *Ultrasonics* 2016; 66: 125–132.
33. Qin N, Pei ZJ, Cong WL, et al. Effects of tool design on edge chipping in ultrasonic-vibration-assisted grinding. In: *Proceedings of the ASME 2010 international manufacturing science and engineering conference*, Erie, PA, 12–15 October 2010, paper no. MSEC2010-34182, pp.147–154. New York: ASME.
34. Jiao Y, Liu WJ, Pei ZJ, et al. Study on edge chipping in rotary ultrasonic machining of ceramics: an integration of designed experiments and finite element method analysis. *J Manuf Sci E: T ASME* 2004; 127: 752–758.
35. Zheng JX and Xu JW. Experimental research on the ground surface quality of creep feed ultrasonic grinding ceramics (Al_2O_3). *Chinese J Aeronaut* 2006; 19: 359–365.
36. Tawakoli T, Azarhoushang B and Rabiey M. Ultrasonic assisted dry grinding of 42CrMo4. *Int J Adv Manuf Tech* 2009; 42: 883–891.
37. Cao JG, Wu YB, Li JY, et al. A grinding force model for ultrasonic assisted internal grinding (UAIG) of SiC ceramics. *Int J Adv Manuf Tech* 2015; 81: 875–885.
38. Liang ZQ, Wu YB, Wang XB, et al. A new two-dimensional ultrasonic assisted grinding (2D-UAG) method and its fundamental performance in monocrystal silicon machining. *Int J Mach Tool Manu* 2010; 50: 728–736.
39. Nik MG, Movahhedy MR and Akbari J. Ultrasonic-assisted grinding of Ti6Al4V alloy. *Proced CIRP* 2012; 1: 353–358 (also published in *fifth CIRP conference on high performance cutting*).
40. Chen HF, Tang JY and Zhou W. An experimental study of the effects of ultrasonic vibration on grinding surface roughness of C45 carbon steel. *Int J Adv Manuf Tech* 2013; 68, 2095–2098.
41. Liu SL, Chen T and Wu CQ. Rotary ultrasonic face grinding of carbon fiber reinforced plastic (CFRP): a study on cutting force model. *Int J Adv Manuf Tech*. Epub ahead of print 12 July 2016. DOI: 10.1007/s00170-016-9151-x.
42. Pei ZJ and Ferreira PM. Modeling of ductile mode material removal in rotary ultrasonic machining. *Int J Mach Tool Manu* 1998; 38: 1399–1418.
43. Marinescu ID, Rowe WB, Dimitrov B, et al. *Tribology of abrasive machining processes*. Norwich, NY: William Andrew Publishing, 2004.
44. Kwak JS and Kim YS. Mechanical properties and grinding performance on aluminum-based metal matrix. *J Mater Process Tech* 2008; 201: 596–600.
45. Xu LF, Zhou L, Yu XL, et al. An experimental study on grinding of SiC/Al composites. *Adv Mat Res* 2011; 188: 90–93.
46. Tawakoli T and Azarhoushang B. Intermittent grinding of ceramic matrix composites (CMCs) utilizing a developed segmented wheel. *Int J Mach Tool Manu* 2011; 51: 112–119.
47. Marinescu ID, Hitchiner M, Uhlmann E, et al. *Handbook of machining with grinding wheels*. Boca Raton, FL: Taylor & Francis Group, 2007.
48. Bhaduri D, Soo SL, Novovic D, et al. Ultrasonic assisted creep feed grinding of Inconel 718. *Proced CIRP* 2013; 6: 615–620 (also published in *proceedings of the seventeenth CIRP conference on electro physical and chemical machining (ISEM)*).
49. McKee RL. *Machining with abrasives*. New York: Van Nostrand Reinhold Company, 1982.
50. Denkena B, Köhler J and Hahmann D. Grinding of steel-ceramic-composites. *Adv Mat Res* 2011; 325: 116–121.
51. Cong WL, Pei ZJ, Churi NJ, et al. Rotary ultrasonic machining of stainless steel: design of experiments. *Trans North Am Manuf Res Inst SME* 2009; 37: 261–268.
52. Cong WL, Pei ZJ, Deines TW, et al. Rotary ultrasonic machining of stainless steels: empirical study of machining variables. *Int J Manuf Res* 2010; 5: 370–386.
53. Jia ZY, Su YL, Niu B, et al. The interaction between the cutting force and induced sub-surface damage in machining of carbon fiber-reinforced plastics. *J Reinf Plast Comp*. Epub ahead of print 7 March 2016. DOI: 10.1177/0731684415626284.
54. Pei ZJ, Khanna N and Ferreira P. Rotary ultrasonic machining of structural ceramics: a review. *Ceram Eng Sci Proc* 1995; 16: 259–278.
55. Pei ZJ, Prabhakar D, Ferreira P, et al. Mechanistic approach to the prediction of material removal rates in rotary ultrasonic machining. *J Eng Ind* 1995; 177: 142–151.

56. Pei ZJ, Prabhakar D, Ferreira P, et al. Rotary ultrasonic drilling and milling of ceramics. In: Hiremath BV, Bruce AJ and Ghosh A (eds) *Manufacture of ceramic components* (vol. 49 of ceramic transactions). Westerville, OH: American Ceramic Society, 1995, pp.185–196.
57. Li ZC, Treadwell C and Pei ZJ. *Drilling small holes in hard to machine materials by rotary ultrasonic machining*. Technical paper TP04PUB137, 28 April 2004. Dearborn, MI: Society of Manufacturing Engineers.
58. Churi NJ, Pei ZJ and Treadwell C. Rotary ultrasonic machining of titanium alloy (Ti-6Al-4V): effects of tool variables. *Int J Precis Tech* 2007; 1: 85–96.
59. Li JG, Du JG and Zhao H. Experimental study on the surface roughness with mill-grinding SiC particle reinforced aluminum matrix composites. *Adv Mat Res* 2011; 188: 203–207.
60. Shi YS, Wang YG, Lin B, et al. Experimental investigation on grinding-induced surface damage of fiber reinforced ceramic matrix composites. *Appl Mech Mater* 2010; 37–38: 424–427.
61. Jia ZY, Fu R, Wang FJ, et al. Temperature effects in end milling carbon fiber reinforced polymer composites. *Polym Composite*. Epub ahead of print 1 March 2016. DOI: 10.1002/pc.23954.